Two-dimensional islanding atop stressed solid helium and epitaxial films

Michael Grinfeld
Department of Mathematics, Rutgers University, New Brunswick, New Jersey 08903
(Received 26 July 1993; revised manuscript received 27 October 1993)

We discuss the role of stress in destabilizing flat surfaces of thin solid films. The presence of this instability in stressed ^{4}He and several heteroepitaxial films is widely acknowledged and well documented. We pay special attention to the study of possible in-plane morphologies of the islands which appear as a result of the stress-driven destabilization of flat traction-free interfaces. We also discuss the critical thickness at which these morphologies change.

I. INTRODUCTION

For many decades morphological instabilities of interfaces have been intensively studied. Traditionally, morphological instabilities have been of primary interest in crystal growth, metallurgy, fracture, geology, petrology, etc. Within the past few years this list has been extended into several new areas, including epitaxy, electronic packaging, tribology, biology, etc. (see, reviews[1–4] and references therein).

Recent efforts by many researchers have resulted in rapid progress and the development of much deeper understanding of the specific stress-driven"rearrangement" instabilities of inclusions, interfaces, and free boundaries in solids, in particular of different phase boundaries.[5] Of the numerous purely energetic instabilities of this sort—the instability of the "stressed crystal–melt" system—has attracted the most attention because of its universal character, its most promising and wide applications, and its apparent simplicity for experimental observation. The instability of stressed crystal—melt system is close to the instability of a stressed solid with respect to surface diffusion along a traction-free boundary,[6] the relationship has remained unnoticed until recently. Although the study of diffusion requires the ideas and methodology of irreversible thermodynamics, the instability studied by Asaro and Tiller[6] is purely energetic in nature as well.

At present, the roots of the stress-driven rearrangement instability have become quite transparent. Several authors[7–10] have demonstrated, using different approaches, that, regardless of specific symmetry, geometry and elastic moduli, accumulated elastic (either linear or nonlinear) energy can always be reduced by means of appropriate mass rearrangement in the vicinity of the free surface. Thus, neglecting surface energy, all nonhydrostatically stressed solids, bounded by a smooth, traction-free boundary, are unstable against appropriate mass rearrangement of their constituent particles. The specific features of the stress-driven rearrangement instabilities depend on geometry, presence of other bodies and forces, mass transport mechanisms, etc. The above statement provides a universal means to more specific predictions of the stress-driven destabilization of traction-free surfaces. We mention, among other features, the instabilities of stressed solids against surface diffusion,[6] of the phase boundary between stressed solid and its melt,[11] and several other instabilities of similar nature.[5] Recently, the instability of the phase boundary separating melted and uniaxially stressed crystalline^4 He has been observed in quantitative experiments by Thiel *et al.*[12] and Torii and Balibar;[13] the stress-driven rearrangement instability fed by diffusion also has been evidenced in a publication by Berrehar *et al.*[14]

Because of its universal nature, the stress-driven "rearrangement" instability provides insights into phenomena in different branches of materials and other sciences, part of which was discussed in Ref. 7. While this stress-driven morphological instability has found widespread applications in different fields (see, for instance, the discussions of the stressed solid–melt instability in the problems of pattern formation in metallurgy,[15] theory of gels,[16] geology,[17] and fracture[18]), it has also received serious attention in problems related to the growth of epitaxial films.[9,19] The reason for this interest can be traced to some recent observations[20] of dislocation-free Stranski-Krastanov growth. These experiments have demonstrated clearly that the Stranski-Krastanov pattern may not be triggered by nucleation of misfit dislocations—as many had previously thought[21]–and hence demands a different approach. The key roles played by misfit stresses and mass rearrangement in this phenomenon were discussed in the past by several authors exploiting different approaches.[22] The most interesting parameters in the problems of epitaxy are those critical thicknesses at which the surface morphology undergoes sudden qualitative changes.

In this paper we treat the phenomena relating to the experiments with prestressed ^{4}He films and the observations on the dislocation-free Stranski-Krastanov growth from the viewpoint of the stress-driven rearrangement instability. We pay special attention to the two-dimensional (2D) in-plane morphologies and their changes at critical thicknesses of the film and/or critical misfit or applied stresses. We also address the role of mass forces, following the lectures and publication of Nozieres.[23]

II. INTUITIVE ANALYSIS OF MECHANISM OF STRESS-DRIVEN REARRANGEMENT INSTABILITY

Let us consider the processes of crystallization of sublimation at the free surface of a uniaxially prestressed,

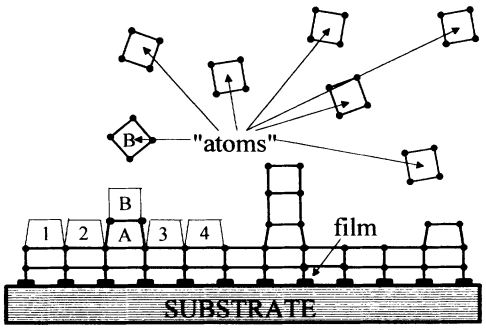

FIG. 1. The mechanism of the stress-driven rearrangement instability.

elastic crystal (see Fig. 1). We explicitly consider three physical effects, namely elasticity, gravity, and surface energy. The stresses within the solid can be generated by an applied stress or be internal stresses, such as those associated with heteroepitaxy. For the sake of simplicity, we consider that the solid is only two-dimensional, and assume that deposition takes place in the form of elementary square cells of material, as per Fig. 1. Assume that the material being deposited has a different lattice parameter from the substrate due to the presence of the uniaxial, lateral stress. When cell A attaches to the uniform adlayer under it, its bottom stretches to match the lattice parameter of the strained adlayer. Its top, on the other hand, remains at its initial unstrained width, and the initially rectangular cell distorts into a trapezoidal shape.

Consider now the possible locations for cell B to attach to the film in the vicinity of cell A. Particle B may attach itself to the adlayer in, e.g., positions 1, 2, 3, or 4. "Normal" gravity favors cell B to attach at the lowest possible position (sites 1, 2, 3, and 4 are all equivalent from this point of view, and they are preferable to the site on top of particle A). Since surface energy favors as large a number of nearest neighbors as possible, sites 2 and 3 are preferable to 1 to 4 due to the proximity of cell A. This is why gravity and surface energy favor the growth of as smooth of a surface as possible. If cell B attaches to site 1 or 4, it will take on the strained, trapezoidal shape of cell A. If, on the other hand, it attaches to site 2 or 3, the wall B shares with A becomes vertical and therefore both cells A and B become more strained than if cell B was at either site 1 or 4. Therefore, strain energy works against the surface smoothing tendencies of the surface energy. Now, consider cell B becoming attached to site B, on top of A. Since site B has the same number of nearest neighbors as sites 1 and 4, the surface energy associated with B is the same for attachment to sites 1, 4, or B. However, while the bottom of cell B would be stretched at sites 1 or 4, its bottom is unstretched at site B because of the top of cell A is unstretched. Therefore, consideration of strain energy favors site B over sites 1–4. This is the stress-driven morphological instability countered by gravity and surface tension.

III. THE "MISFIT" DEFORMATION AND STRESS

Let us consider an elastic solid substance with elastic energy density $e(\varepsilon_{ij})$ per unit volume in the initial unstressed state; $\varepsilon_{ij}=(D_j u_i+D_i u_j)/2$ is the dependence of the linear deformation tensor on the displacements gradient; D_i is the symbol of differentiation with respect to the Lagrangian (material) coordinates x^i (the Latin spatial indexes i, j, k, and l take on the values of 1, 2, and 3, whereas the initial Latin indexes a, b, c, and d are either 1 or 2), and the Einstein convention (summation over repeated indexes–e.g., $\kappa_1^i=\kappa_1^1+\kappa_2^2+\kappa_3^3$, $\kappa_c^c=\kappa_1^1+\kappa_2^2$) is implied.

Consider an elastic, crystalline solid in the form of a relatively thin layer (film) which is coherently attached to a solid crystalline substrate modeled as the half-space (see Fig. 2). The interface is initially flat. We examine the cases of a rigid or deformable substrate. The interface can be viewed as a perfect plane possessing the 2D lattice of atoms. Because of the mismatch in the lattice parameters between the unstressed crystalline film and the substrate, the 2D interface lattice of atoms of the film is subjected to the in-plane "misfit" deformation M^2. Choosing the coordinate system with the (x^1,x^2) plane coinciding with the interface, one can express the affine misfit displacements in the film as

$$U_a(x^b)=\kappa_{ab}x^b \quad [\text{or } U_1(x^1,x^2)=\kappa_{11}x^1+\kappa_{12}x^2,\quad U_2(x^1,x^2)=\kappa_{21}x^1+\kappa_{22}x^2] , \tag{1}$$

where κ_{ab} is the 2D tensor defined by the in-plane lattices (as we use the Cartesian coordinates only, there are no distinctions in the covariant and contravariant components). Thus the in-plane components of the 3D displacements of film $u^i(x^j)$ should obey the interface Γ $(x^3=0)$:

$$\begin{aligned} &u_1(x^1,x^2,0)=\kappa_{11}x^1+\kappa_{12}x^2 , \\ &u_2(x^1,x^2,0)=\kappa_{21}x^1+\kappa_{22}x^2 , \\ &u_3(x^1,x^2,0)=0 \quad [\text{or } u_a(x^b,0)=U_a(x^b)=\kappa_{ab}x^b] . \end{aligned} \tag{2}$$

So far we have dealt with in-plane components of the misfit deformation κ_{ab} only. However, it is convenient to extend our original notion of the 2D misfit deformations M^2 to the 3D misfit deformation, with the components κ_{ij} defined in the following way. Let us consider the equilibrium displacements of the unbounded elastic layer with a traction-free and perfectly flat surface and flat interface where the film is coherently attached to the substrate. The lattice misfit M^2 generates 3D uniform strains and stresses within the film. We identify the components as the 3D misfit strain and stress, with tensors κ_{ij} and p^{ij0}, respectively. The indices of components κ_{ij} running over 1 and 2 are obviously equal to the components of the 2D misfit deformation κ_{ab}. Since all material particles of any arbitrary horizontal plane of the film experience the same vertical displacement in the 3D misfit deformation, the

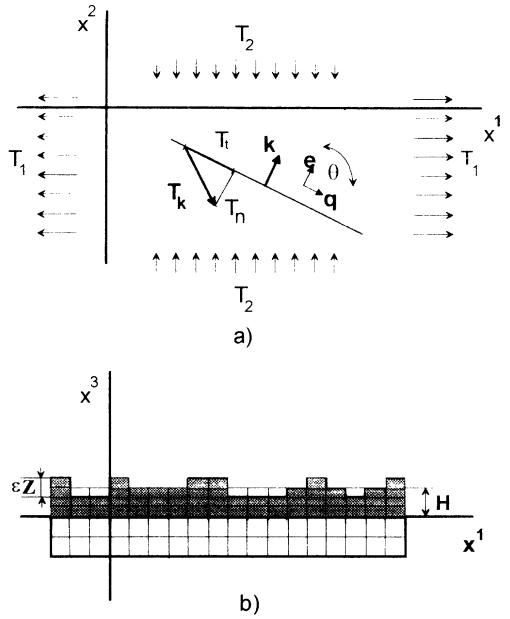

FIG. 2. The geometry of the corrugated film. (a) Top view. (b) Side view.

components κ_{31} and κ_{32} vanish identically in crystals of any symmetry. The three remaining components κ_{i3} should guarantee the absence of traction at the free surface (and, because of uniformity, at the interface as well): $p^{3j0}=p^{i30}=0$. These algebraic equations can be rewritten in terms of the elastic constant tensor as $c^{i3kl}\kappa_{kl}=0$. The misfit strains and stresses can easily be computed for the case of an isotropic elastic solid. In this case, the elastic constant tensor is simply $c^{ijkl}=\lambda\delta^{ij}\delta^{kl}+\mu(\delta^{ik}\delta^{jl}+\delta^{il}\delta^{jk})$, where λ and μ are the Lame constants and δ_{ij} is the Kronecker delta function. Simple manipulations lead to the following components of the misfit strain and stress:

$$\kappa_{a3}=0,\kappa_{33}=-\frac{\nu}{1-\nu}\kappa_a^a\ ,\qquad p^{ab0}=2\mu\left[\frac{\nu}{1-\nu}\kappa_c^c\delta^{ab}+\kappa^{(ab)}\right],\quad p^{j3\sigma}=p^{3j0}=0\ , \tag{3}$$

where ν is the Poisson ratio, and $\kappa^{(ab)}=(\kappa^{ab}+\kappa^{ba})/2$ is the symbol for symmetrization.

In the following sections, we use the notation T_1 and T_2 for the principal in-plane misfit stress (i.e., the eigenvalues of stresses p^{ab0}) and choose the principal in-plane directions (i.e., the eigenvectors) as the x^1 and x^2 axes. We refer to "shearlike" misfit stresses when T_1 is approximately $-T_2$, and as "dilatationlike" misfit stresses when T_1 is approximately T_2.

IV. THE ELASTIC ENERGY ASSOCIATED WITH CORRUGATIONS OF THE FILM SURFACE

Here, we follow lectures[8] and the latter of Ref. 7. Consider the "uncorrugated" (i.e., flat) elastic film with a free surface at $x^3=H$, which is coherently attached to an infinitely thick elastic substrate at $x^3=0$. The infinitely thick substrate is stress free and has zero strain energy, while the film is subjected to the misfit strain κ_{ij} and therefore has a nonzero elastic energy $E_{\rm reg}$ proportional to its volume ω^0 and the elastic energy density $e_{\rm reg}=\frac{1}{2}c^{ijkl}\kappa_{ij}\kappa_{kl}$. Imagine that the free surface of the film γ becomes "corrugated" via rearrangement of the material particles. The amplitude of the corrugation $\varepsilon Z(x^a)$ is assumed to be sufficiently small in the sense that the corrugated surface γ^ε is close to the original surface γ^0:

$$\gamma^\varepsilon: x^3=H+\varepsilon Z(x^a),\quad \varepsilon\ll 1\ , \tag{4a}$$

$$\int_\gamma dx^1dx^2Z(x^a)=0\ . \tag{4b}$$

Equation (4b) reflects conservation of the film mass. We denote the equilibrium displacement field and the accumulated elastic energy of the system with the corrugated, traction-free surface γ as $u_i(x^k,\varepsilon)$ and $E^e_{\rm irreg}(\varepsilon)$, respectively. Expanding $u_i(x^k,\varepsilon)$ and $E^e_{\rm irreg}(\varepsilon)$ in series of ε, and inserting them into equilibrium equations and boundary conditions, we find the following central formula:[7]

$$E^e_{\rm irreg}(\varepsilon)-E^e_{\rm reg}(\varepsilon)\cong-\frac{\varepsilon^2}{2}\int_{\omega_0}d\omega\,c^{ijkl}D_{(j}v_{i)}D_{(i}v_{k)}\ . \tag{5}$$

Here $v_i(x^k)$ is the disturbance of the equilibrium displacement field $u_i=\kappa_{ij}x^j+\varepsilon v_i(x^k)$; it should satisfy the following equations:

$$\begin{aligned}&c^{ijkl}D_jD_lv_k=0\ \text{ within the film and deformable substrate,}\\ &v_k=0\ \ ([v_k]^+_-=0)\ \text{ at the interface }\Gamma\ ,\\ &c^{ijkl}D_{(l}v_{k)}n_j=\delta^i_bp^{ab0}D_aZ\ \text{ at the undisturbed traction-free boundary }\gamma^0\ .\end{aligned} \tag{6}$$

The right-hand side of (6_3) appears because of the change of the free boundary position; $[v_k]^+_-$ is the jump at the matching surface.

Equation (5) shows that any corrugations of the initially flat, traction-free surface diminish the total strain energy of the system.

Integration in Eq. (5) expands over both solids: over the film and the substrate since the corrugations induce stresses in the substrate as well. Combining Eqs. (5) and (6), we arrive at the following 3D generalization of the formula established by Nozieres[8] (which is very convenient for the computation):

$$E^e_{\rm irreg}(\varepsilon)-E^e_{\rm reg}(\varepsilon)\cong-\frac{\varepsilon^2}{2}p^{ab0}\int_{\gamma^0}d\gamma\,v_bD_aZ\ . \tag{7}$$

Consider now isotropic substances; Eqs. (6) can be rewritten in the bulk as

$$\frac{\partial}{\partial x^a}\frac{\partial v^b}{\partial x^b}+(1-2\nu)\left[\Delta_s v_a+\frac{\partial^2 v_a}{\partial z^2}\right]+\frac{\partial^2 v^3}{\partial x^a \partial_z}=0\ ,$$
$$2(1-\nu)\frac{\partial^2 v^3}{\partial z^2}+(1-2\nu)\Delta_s v^3+\frac{\partial^2 v^a}{\partial x^a \partial z}=0\ , \tag{8a}$$

at the interface Γ of the rigid (deformable) substrate as

$$v_k=0\quad([v_k]^{+}_{-}=0)\ , \tag{8b}$$

and at the free surface γ^0 as

$$\frac{\partial v_a}{\partial z}+\frac{\partial v^3}{\partial x^a}-\tau^{ab}\frac{\partial Z}{\partial x^b}=0\ ,$$
$$(1-\nu_f)\frac{\partial v^3}{\partial z}+\nu_f\frac{\partial v^a}{\partial x^a}=0\ , \tag{8c}$$

where ν_f is the Poisson ratio, $\tau^{ab}=p^{ab0}/\mu_f$ are the nondimensional misfit stresses, and μ_f is the shear module of the adlayer.

We look for the Fourier solution of Eqs. (8):

$$Z(x^a)=\int_{R^2} dk_1 dk_2 \Delta(k_1,k_2)e^{ik_a x^a}\ ,$$
$$v_i(x^j)=\int_{R^2} dk_1 dk_2 v_{iF}(k_1,k_2,z)e^{ik_a x^a}\ ,$$

where $\mathbf{k}(k_a)$ is the in-plane wave vector of the corrugations. The bulk Eq. (8a) lead to the following formulas for u_{iF}:

$$v_{3F}=Q_+e^{|\mathbf{k}|z}+R_+ze^{|\mathbf{k}|z}+Q_-e^{-|\mathbf{k}|z}+R_-ze^{-|\mathbf{k}|z}\ ,$$
$$v^a(z)=i\frac{k^a}{|\mathbf{k}|^2}\{[Q_+|k|+R_+(3-4\nu)]e^{|\mathbf{k}|z}+R_+|\mathbf{k}|e^{|\mathbf{k}|z}$$
$$-[-Q_+|\mathbf{k}|+R_-(3-4\nu)]e^{-|\mathbf{k}|z}-R_-|\mathbf{k}|ze^{-|\mathbf{k}|z}\}+iq^a(T_+e^{|\mathbf{k}|z}+T_-e^{-|\mathbf{k}|z})\ , \tag{9}$$

where $Q_\pm$, $R_\pm$, and $T_\pm$ are constants, whereas $\mathbf{q}(q^a)$ is the in-plane unit vector orthogonal $\mathbf{k}$. The constants can be computed with the help of Eqs. (8b) and (8c). Then, using (6), one can find an elastic energy release caused by corrugating. This computation can be made more explicit by considering an isotropic elastic film and substrate. Omitting the mathematical details, we find

$$E^e_{\text{irreg}}-E^3_{\text{reg}}=\varepsilon^2\int_{-\infty}^{\infty}\int_{-\infty}^{\infty}\mathbf{K}_e\Delta(\mathbf{k})\Delta^*(-\mathbf{k})dk_1dk_2\ , \tag{10}$$

where

$$\mathbf{K}_e=-\frac{|\mathbf{k}|}{2\mu_f}\left\{\frac{1-\nu_f}{\Pi}\left[h-\tfrac{1}{2}\sinh 2h\left[1+\frac{4(1-\nu_f)[\chi(1-2\nu_s)+1]}{(\chi-1)[\chi(3-4\nu_s)+1]}\right]\right.\right.$$
$$\left.\left.-\cosh 2h\frac{4\chi(1-\nu_f)(1-\nu_s)}{(\chi-1)[\chi(3-4\nu_s)+1]}\right]T_n^2+\frac{\sinh h+\chi\cosh h}{\cosh+\chi\sinh h}T_t^2\right\}\ ,$$
$$\Pi=h^2-\frac{1}{(\chi-1)[\chi(3-4\nu_s)+1]}[\chi\sinh h+\cosh h+(1-2\nu_f)(\sinh h+\cosh h)]$$
$$\times[\chi\sinh h+\cosh h+(1-2\nu_f)(-\sinh h+\cosh h)+2\chi(1-2\nu_s)\sinh h]\ .$$

The following notation has been employed in Eq. (10): μ_f, ν_f, μ_s, and ν_s are the shear moduli and Poisson ratios of the film and substrate, respectively ($\chi=\mu_f/\mu_s$); θ is the angle between $\mathbf{k}$ and the principal direction of the in-plane stress T_1; $\mathbf{e}$ and $\mathbf{q}$ are the unit in-plane vectors parallel and orthogonal to $\mathbf{k}$, respectively; T_n ($=T_1e_1^2+T_2e_2^2=T_1\cos^2\theta+T_2\sin^2\theta$) and T_t [$=T^1e_1q_1+T^2e_2q_2=(T_1-T_2)\sin\theta\cos\theta$] are the normal and tangential components of the stress $\mathbf{T}_\mathbf{k}$ acting at the cross section orthogonal to the wave vector $\mathbf{k}$; the number $h=|\mathbf{k}|H$ can be treated as a dimensionless wave vector or film thickness.

V. THE ENERGY BALANCE OF ELASTIC SYSTEMS WITH REARRANGEMENT AND THEIR MORPHOLOGICAL STABILITY

In addition to the elastic energy, the surface E_s and potential energy E_g also make contributions to the total energy of the film-substrate systems. The force field is assumed to be one dimensional; the acceleration g depends on the distance from the substrate. The surface energy is assumed to be proportional to the product of the surface energy density σ and the total area of the free surface in the stress-free reference configuration. We explicitly neglect the contribution of the surface stress to the elastic energy.[20] The change E^t_{irreg}-E^t_{reg} in total energy associated with the formation of surface corrugation on an initially flat surface is

$$E^t_{\text{irreg}}-E^t_{\text{reg}}=\varepsilon^2\int_{-\infty}^{+\infty}dk_1\int_{-\infty}^{+\infty}dk_2\mathbf{K}(\mathbf{k},H)\Delta(\mathbf{k})\Delta^*(-\mathbf{k})\ , \tag{11}$$

which can be computed explicitly for isotropic substances.

The function $\mathbf{K}(\mathbf{k},H)$ includes (i) the potential energy K_g; (ii) the bulk (elastic) energy K_b; and (iii) the surface

energy K_s, which, to within an insignificant positive multiplier, is

$$\mathbf{K}(\mathbf{k},H)=K_g+K_b+K_s$$
$$=g\rho_v(\gamma-1)-|\mathbf{k}|J_b(\mathbf{e},h)+\sigma|\mathbf{k}|^2 , \quad (12)$$

where $\gamma=\rho_s/\rho_v$ is the density ratio of the solid film and the melt. In the case of epitaxial film we insert $g\rho_s$ for $g\rho_v(\gamma-1)$ to account for the van der Waals forces.[23] Though van der Waals forces play a significant role in the behavior of polymeric films, it should be noted that these forces depend strongly on the distance from the substrate. On the other hand, there are several indications that in Se-Ge and other semiconductor heteroepitaxial composites the interactions between the films and substrates are of a localized, covalent nature due to the formation of strong covalent bonds. This is a qualitatively different interaction than van der Waals forces. Therefore, our analysis of the role of mass forces presumably cannot be applied to semiconductor films.

In contrast to the potential and surface energies the bulk energy term $J_b(\mathbf{e},h)$ depends on the mechanical properties of the film and substrate, and of their thicknesses.

We can label all types of corrugations as either stable, neutral, or destabilizing depending on their wave vector, the nature of the stress field, and the physical properties of the materials. We find the following conditions for stability, neutrality, or instability:

$$\mathbf{K}(\mathbf{k},H)>0, \quad \mathbf{K}(\mathbf{k}_{ne},H)=0, \quad \mathbf{K}(\mathbf{k},H)<0 , \quad (13)$$

respectively. Corrugations which are unstable grow in amplitude; corrugations which are stable decay in amplitude and neutral corrugations neither grow nor shrink. A film thickness for which all corrugations are stable is referred to as stable. Situations in which at least one destabilizing corrugation exist are unstable. The critical thickness of the uniform film corresponds to the situation in which there are no destabilizing corrugations, and for which at least one mode of surface corrugation is neutral. The corrugations with a wave vector $\mathbf{k}$ that minimizes K are maximally unstable. In other words, this is the corrugation wave vector which decreases the energy of the system with increasing amplitude faster than corrugation of any other wave vector. This is the corrugation wave vector that will likely dominate the surface morphology. However, different material transport mechanisms may shift the fastest-growing corrugation to nearby wave vectors. The function $G\equiv -K$ is proportional (in a certain range of $\mathbf{k}$ vectors) to the (quasistatic) rate of growth of the Fourier component of the configurations.

VI. MORPHOLOGICAL PATTERNS ATOP THE FILMS BONDED TO A RIGID SUBSTRATE

The approximation of a rigid substrate seems reasonable when dealing with very soft crystalline ^{4}He. We first consider the case of a film attached to a rigid substrate ($\nu_s=\frac{1}{2}$, $\chi=0$) in the absence of gravity. Then, this case, Eqs. (10)–(12) yield

$$G(\mathbf{k},H)=-\sigma|\mathbf{k}|^2+\frac{|\mathbf{k}|}{\mu_f}\left[\frac{(1-\nu_f)[h+(3-4\nu_f)\sinh h\cosh h]}{4(1-\nu_f)^2+h^2+(3-4\nu_f)\sinh^2 h}T_n^2+\frac{\sinh h}{\cosh h}T_t^2\right] . \quad (14)$$

Introducing the angle θ between $\mathbf{e}$ and the principal in-plane stress, T_1, Eq. (14) can be rewritten as ($\tau_a=T_a/\mu_f$ are the dimensionless principal in-plane stresses)

$$\frac{4G}{\mu_f|\mathbf{k}|(\tau_1-\tau_2)^2}=-A+B\sin^2 2\theta+C(s+\cos 2\theta)^2 , \quad (15)$$

where

$$A=\frac{4\sigma|\mathbf{k}|}{\mu_f(\tau_1-\tau_2)^2}, \quad B=\frac{\sinh h}{\cosh h} ,$$
$$C=\frac{(1-\nu_f)[h+(3-4\nu_f)\sinh h\cosh h]}{4(1-\nu_f)^2+h^2+(3-4\nu_f)\sinh^2 h} ,$$
$$s=\frac{\tau_1+\tau_2}{\tau_1-\tau_2} .$$

The dimensionless parameter s characterizes the in-plane misfit stresses, and it plays a crucial role in determining the dominant surface morphology; s equals to ± 1 in the case of uniaxial stress, vanishes for pure in-plane shear, and is infinite for pure in-plane dilatation. The surface energy term in Eq. (14) prevails at $|\mathbf{k}|$ approaching infinity and, thus, corrugations with sufficiently small wavelength always raise the total accumulated energy of the system. In order for long-wavelength corrugations ($|\mathbf{k}|\ll 1$) to be stable, the function $\mathbf{K}$ (G) must be positive (negative). In that range Eq. (15) can be rewritten as

$$\frac{4G}{\mu_f|\mathbf{k}|(\tau_1-\tau_2)^2}\sim -\frac{4\sigma}{\mu_f(\tau_1-\tau_2)^2}$$
$$+H(1+2s\cos 2\theta+s^2) . \quad (16)$$

The right-hand side of Eq. (16) reaches maximum at $\cos 2\theta=1$ or $\cos 2\theta=-1$ (whichever is greater). We assume that $|\tau_1|>|\tau_2|$ (it can be always achieved by changing enumeration). Then the maximum of $4(\tau_1-\tau_2)^2(H\tau_1^2-\sigma\mu_f^{-1})$ is assumed at $\theta=0$. That circumstance leads to the following formula for the first critical thickness (Grinfeld[5,7,19] and Spencer and coworkers[19]):

$$H_{\text{crit}}=\frac{\sigma}{\mu_f\tau_1^2}=\frac{\sigma\mu_f}{T_1^2} \quad (17)$$

above which the free surface becomes rough.

We now examine the extrema on the right-hand side of

Eq. (15), which we denote as $\varphi(\theta)$. Setting the first derivative of $\varphi(\theta)$ to zero, we find that there are two types of extrema satisfying

$$\text{(a) } \sin 2\theta = 0 \text{ and (b) } \cos 2\theta = \frac{C}{B-C}s \ . \tag{18}$$

The "a" solutions always exist, and correspond to $\mathbf{k}$ vectors which are parallel to the directions of the lateral principal stresses (i.e., corrugations with a valley perpendicular to the directions of the lateral principal stresses). The "b" solutions may or may not exist, depending on whether the inequality

$$-1 \le \frac{C}{B-C}s \le 1 \tag{19}$$

is satisfied.

Second derivatives of $\varphi(\theta)$ allows us to investigate stability:

$$\varphi'' = 8(B-C)\left[1 \pm \frac{C}{B-C}s\right]$$

for the "a" solutions , (20a)

$$\varphi'' = -8(B-C)\sin^2 2\theta \quad \text{for the "b" solutions,} \tag{20b}$$

where the plus sign in (20a) corresponds to the k vector parallel to the x^1 axis, whereas the minus corresponds to the k vector parallel to the x^2 axis. The function G assumes the following values for "a" and "b" solutions:

$$\frac{4G^a_{\text{extr}}}{\mu_f |\mathbf{k}|(\tau_1-\tau_2)^2} = -A + C(s \pm 1)^2$$

for the "a" solutions , (20c)

$$\frac{4G^b_{extr}}{\mu_f |\mathbf{k}|(\tau_1-\tau_2)^2} = -A + B + \frac{BC}{B-C}s^2$$

for the "b" solutions. (20d)

According to Eqs. (18)–(20), one of the "a" solutions gives the maximum value of $\varphi(\theta)$, whereas the other corresponds to minimum values of $\varphi(\theta)$, provided that "b" solutions do not exist [because of the violation of the inequalities (19)]. If "b" solutions do exist and $B > C$, then, according to Eqs. (20c) and (20d) "b" solutions correspond to maxima in $\varphi(\theta)$, whereas "a" solutions deliver $\varphi(\theta)$ minima [if $B < C$, then the situation is opposite: "b" solutions yield maximum of $\varphi(\theta)$]. It is obvious that at fixed $|\mathbf{k}|$ and h the solutions maximizing φ determine the most probable surface morphology. "b" solutions exist for "shearlike" misfit stresses, but and do not exist at the "dilatationlike" misfit stresses. In order to make these results more concrete, we now consider several specific applications of these results.

Certain special cases

1. *Pure in-plane dilatation*

In this case, the principal in-plane stresses are equal, i.e., $\tau_1 = \tau_2 = \tau$. As a result, the dimensionless parameter a is infinite and Eq. (15) should be rewritten as

$$G = -\sigma|\mathbf{k}|^2 + C\tau^2\mu_f|\mathbf{k}| \tag{21a}$$

or, in the dimensionless form,

$$\frac{GH}{\mu_f\tau^2} = -\frac{1}{\Phi\alpha^H_{\text{dil}}}h^2 + Ch \quad \text{where } \Phi\alpha^H_{\text{dil}} \equiv \frac{\mu_f\tau^2 H}{\sigma} \ . \tag{21b}$$

Thus, given $h(=H|\mathbf{k}|)$ and $|\mathbf{k}|$, all the Fourier components of the corrugation have the same energy dependence on amplitude, independent of the angle θ.

In the case of the incompressible film Eq. (21a) takes the following form:

$$\frac{GH}{\mu_f\tau^2} = -\frac{1}{\Phi\alpha^H_{\text{dil}}}h^2 + \frac{h}{2}\frac{h + \sinh h \cosh h}{h^2 + \cosh^2 h} \ . \tag{22}$$

Several plots of the right-hand side of Eq. (22) are shown in Fig. 3. Positive maxima of these plots (existing for all $\Phi\alpha^H_{\text{dil}}$ exceeding 1) depend on the value of $\Phi\alpha^H_{\text{dil}}$.

Another form of Eq. (21) is more convenient for an infinitely thick layer:

$$\frac{G}{\mu_f\tau^2} = \left[-\frac{1}{\Phi\alpha^k_{\text{dil}}} + 1 - \nu_f\right]k \quad \text{where } \Phi\alpha^k_{\text{dil}} \equiv \frac{\mu_f\tau^2}{\sigma|\mathbf{k}|} \ . \tag{23}$$

Equation (23) shows that the wave numbers $|\mathbf{k}|_{\text{ne}}$ and $|\mathbf{k}|_p$ corresponding to the neutral and most probable corrugations (at which the G function vanishes and reaches its maximum, respectively) are

$$|\mathbf{k}|_{\text{ne}} = (1-\nu_f)\frac{\mu_f\tau^2}{\sigma} \quad \text{or} \quad \Phi\alpha^k_{\text{dil ne}} = \frac{1}{1-\nu_f} \ ,$$
$$|\mathbf{k}|_p = \tfrac{1}{2}(1-\nu_f)\frac{\mu_f\tau^2}{\sigma} \ . \tag{24}$$

2. *Pure in-plane shear*

In this case, the principal in-plane stresses are of the same absolute value and of opposite sign: $\tau_1 = -\tau_2 = \tau$. In pure in-plane shear the dimensionless parameter s is zero, such that Eqs. (17) and (18b) can be rewritten as

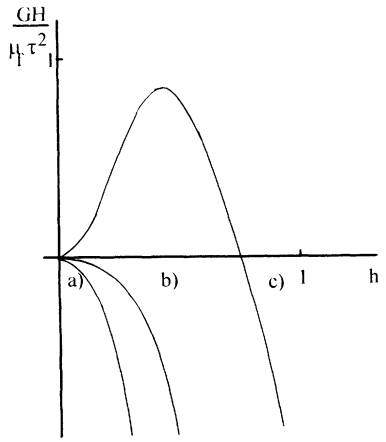

FIG. 3. The dependence of the contributed energy for $h = kH$. (a) $\Phi\alpha^H_{\text{dil}} = \frac{1}{2}$. (b) $\Phi\alpha^H_{\text{dil}} = 1$, (c) $\Phi\alpha^H_{\text{dil}} = 2$.

$$\frac{4G}{\mu_f|\mathbf{k}|\tau^2}=-\frac{\sigma|\mathbf{k}|}{\mu_f\tau^2}+B\sin^2 2\theta+C\cos^2 2\theta\ , \tag{25a}$$

$$\cos 2\theta=0\ . \tag{25b}$$

Equation (25b) shows that "b" solutions always exist in pure shear and have optimal $\mathbf{k}$ vectors bisecting the principal in-plane directions. Equations (25) result in the following extreme values of the G function for "a" and "b" solutions, respectively:

$$\text{(a)}\ \frac{4G^a_{\text{extr}}}{\mu_f|\mathbf{k}|\tau^2}=-A+C,$$

$$\text{(b)}\ \frac{4G^b_{\text{extr}}}{\mu_f|\mathbf{k}|\tau^2}=-A+B$$

$$\left\{\frac{4G^a_{\text{extr}}-4G^b_{\text{extr}}}{\mu_f|\mathbf{k}|\tau^2}=B-C\right\}. \tag{26}$$

In the case of incompressible isotropic film, we arrive at the following inequality:

$$B-C=\frac{4h^2\sinh h+\cosh h(\sinh 2h-2h)}{4\cosh h(h^2+\cosh^2 h)}>0 \tag{27}$$

and, according to Eq. (27), the "b" mode of corrugation is the most probable. For incompressible film Eqs. (26) can be rewritten as

$$\frac{G^a_{\text{extr}}H}{\mu_f\tau^2}=-\Phi\alpha^H_{sh}h^2+\frac{h}{2}\frac{h+\sinh h\cosh h}{h^2+\cosh^2 h} \tag{28a}$$

$$\frac{G^b_{\text{extr}}H}{\mu_f\tau^2}=-\Phi\alpha^H_{sh}h^2+\frac{\sinh h}{\cosh h}\ , \tag{28b}$$

the first of which is identical to Eq. (23). The graphs of the plots of the right-hand side of Eq. (28) are similar to those plotted in Fig. 3.

3. *The infinitely thick film (arbitrary misfit stress)*

According to (17), for infinitely thick film the parameters B and C are equal to 1 and $1-\nu_f$, respectively. Inserting these values into Eq. (21) and considering "a" modes for the corrugations, we find

$$\frac{G^a_{\text{extr}}}{\mu_f(\tau_1-\tau_2)^2}=\left[-\frac{4}{\Phi\alpha^k}+(1-\nu_f)(s\pm 1)^2\right]|\mathbf{k}|$$

$$\text{where}\ \Phi\alpha^k\equiv\frac{\mu_f(\tau_1-\tau_2)^2}{\sigma|\mathbf{k}|}\ , \tag{29}$$

which leads to the following analogs of Eq. (24):

$$|\mathbf{k}|_{ne}=\tfrac{1}{4}(1-\nu_f)(s\pm 1)^2\frac{\mu_f(\tau_1-\tau_2)^2}{\sigma}$$

or (30)

$$\Phi\alpha^k_{ne}=\frac{4}{(1-\nu_f)(s\pm 1)^2}\ ,$$

$$|\mathbf{k}|_p=\tfrac{1}{8}(1-\nu_f)\frac{\mu_f(\tau_1-\tau_2)^2}{\sigma}\ .$$

Equations (30) give the most probable corrugations when "b" modes no not exist. In the case at hand, Eq. (18b) for orientation of the $\mathbf{k}$ vectors, the existence inequality (19) and Eq. (21b) for G^b_{extr} can be reduced to the following forms, respectively:

$$\cos 2\theta=\frac{\nu_f}{1-\nu_f}s,\quad \left|\frac{\nu_f}{1-\nu_f}s\right|<1\ ,$$

$$\frac{4G^b_{\text{extr}}}{\mu_f(\tau_1-\tau_2)^2}=-\frac{4\sigma|\mathbf{k}|^2}{\mu_f(\tau_1-\tau_2)^2}+\left[1+\frac{1-\nu_f}{\nu_f}s^2\right]|\mathbf{k}|\ . \tag{31}$$

4. *The growing film of finite thickness (arbitrary stress)*

The special cases discussed above clearly demonstrate that different patterns of islanding which can occur in even the simplest situation of isotropic incompressible elastic films. Equation (15) can be rewritten in the following dimensionless form:

$$\frac{4GH}{\mu_f(\tau_1-\tau_2)^2}=-\frac{4}{\Phi\alpha^H}h^2+[B\sin^2 2\theta+C(s+\cos 2\theta)^2]h\ , \tag{32}$$

where $\Phi\alpha^H$ equals $\mu_f\sigma^{-1}(\tau_1-\tau_2)H$, and increases with growth of film thickness.

The first term on the right-hand side of (32) is negative, while the second is positive. Regardless of the magnitude of $\Phi\alpha^H$, the first term prevails for a sufficiently large h. Therefore, the G function is negative for a large h. The dimensionless parameter h is proportional to $|\mathbf{k}|$ at a fixed H. Thus, for each fixed thickness, the film is stable with respect to the corrugations of the free surface with sufficiently small wavelengths.

At h approaching zero, Eq. (32) can be rewritten as

$$\frac{4GH}{\mu_f(\tau_1-\tau_2)^2}=\left[1+2\cos 2\theta+s^2-\frac{4}{\Phi\alpha^H}\right]h^2\ . \tag{33}$$

For small fixed h and $|\tau^{-1}|>|\tau^2|$, the right-hand side of Eq. (33) reaches its maximum:

$$\left[(s+1)^2-\frac{4}{\Phi\alpha^H}\right]h^2=\left[\frac{4\tau_1^2}{(\tau_1-\tau_2)^2}-\frac{1}{\Phi\alpha^H}\right] \tag{34}$$

at the angle θ determined by the equation $\cos 2\theta=1$.

The unstable corrugations exist provided that the coefficient of h^2 in (34) is positive; this condition leads to the dimensionless inequality

$$\Phi\alpha^H_{\text{crit}}\le\Phi\alpha^H\ \text{ where }\ \Phi\alpha^H_{\text{crit}}=\frac{4}{(1+s)^2}=\frac{(\tau_1-\tau_2)^2}{\tau_1^2}\ . \tag{35}$$

Thus growing film with flat, free surface and sufficiently small thicknesses is stable against all surface corrugations. Certain corrugations, however, destabilize the free surface if the thickness exceeds the critical magnitude H_{crit}. For that magnitude, the dimensionless number $\Phi\alpha^H$ yields the inequality (35). We say that the film is

slightly unstable when H is slightly larger than $H_{\rm crit}$, and that the $\Phi\alpha^H$ number is slightly larger than $\Phi\alpha^H_{\rm crit}$. Assume now that (i) the parameter s is not equal to zero or infinity (these special cases were already discussed above), and that (ii) the film is slightly unstable. It appears that a periodic system of trenches, which are orthogonal to the direction of the maximal in-plane misfit stress τ_1, are the prevailing pattern of corrugations.

Let us now consider a growing film whose rate of deposition is much faster than the rates of growth of the unstable corrugations. It then seems reasonable to investigate the film's free-surface pattern of small corrugations for a thickness H and a $\Phi\alpha^H$ number much greater than the critical magnitudes. There can be two essentially different scenarios which depend on the misfit stress parameter s and the Poisson ratio ν_f. The first of these occurs if there is no h satisfying the inequality (19); then the system of parallel trenches of one and the same orientation is the dominant pattern of corrugations at each transcritical thickness. The distance between the trenches depends on the magnitude of the $\Phi\alpha^H$ number, and is determined by the maximum of the function

$$\frac{4G^a_{\rm extr}H}{\mu_f(\tau_1-\tau_2)^2}=-\frac{4}{\Phi\alpha^H}h^2+C(s+1)^2h\ . \tag{36}$$

The second scenario occurs if there are positive h's, satisfying the inequality (19). Its existence obviously depends on the function $C/(B-C)$. Several plots of the function $C/(B-C)$ are shown in Fig. 4: the function approaches infinity as h approaches zero. Therefore, the domain of the values h which satisfy Eq. (19) is separated from the origin $h=0$ provided that s differs from zero. This fact shows again that when the film thickness increases, the first unstable corrugations which appear are determined by "a" solutions (corresponding to the system of parallel trenches at the surface); with further thickening, these trenches then change in a fashion similar to that in the first scenario until the second critical magnitude of $\Phi\alpha^H_*$ is reached. At the second critical thickness, the value h^* satisfies the equation

$$\frac{C(h^*)}{B(h^*)-C(h^*)}=1\ . \tag{37}$$

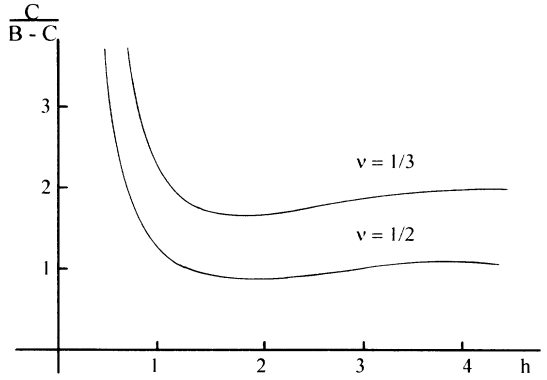

FIG. 4. To the equation of polarization of the wave vector $\mathbf{k}$.

At that thickness, the optimal polarizations of the $\mathbf{k}$ vectors of "a" and "b" solutions coincide. With further growth (at $\Phi\alpha^H>\Phi\alpha^H_*$), the most unstable corrugations switch to the "b" solutions. The length and orientation of the optimal $\mathbf{k}$ vector are now determined by Eqs. (18b) and (21b). According to Fig. 4, "b" solutions for certain ν_f and s can disappear again for some thicknesses, and the morphology switches back to the "a" trenches. For other cases, "b" solutions exist for all $\Phi\alpha^H>\Phi\alpha^H_*$. When $\Phi\alpha^H$ approaches infinity the most probable corrugations approach those described in the third example.

VII. THE INFLUENCE OF MASS FORCES

The interaction of mass rearrangement, gravity, surface energy, and stress in destabilizing phase boundaries and free surfaces in isotropic elastic half-planes has already been studied thoroughly[7,8,18,24] in connection with the instability of the phase boundary separating melted and crystalline ^{4}He. In the following discussion we focus on the role of mass forces in the trenchlike pattern "a" (pattern "b" can be investigated similarly). Pattern "a" permits complete consideration in the framework of 2D elasticity. Equation (12) allows one to compute the critical thickness and neutral wave vector for the arbitrary function $g(H)$. In 2D we can rewrite it as

$$|\mathbf{k}|^{-1}\Gamma^*+|\mathbf{k}|\Sigma^*=\frac{(1-\nu_f)[|\mathbf{k}|H+(3-4\nu_f)\sinh(|\mathbf{k}|H)\cosh(|\mathbf{k}|H)]}{4(1-\nu_f)^2+(|\mathbf{k}|H)^2+(3-4\nu_f)\sinh^2(|\mathbf{k}|H)} \tag{38}$$

using dimensionless parameters Γ^* and Σ^*.

$$\Gamma^*=\frac{g\rho_v(\gamma-1)\mu_f}{T_1^2}=\frac{g\rho_s\mu_f}{\gamma T_1^2},\quad \Sigma^*=\frac{\sigma\mu_f}{T_1^2}\ . \tag{39}$$

For positive $\Gamma^*(H)$, the left-hand side of Eq. (38) reaches the minimum $2\sqrt{\Gamma^*\Sigma^*}$ at $|\mathbf{k}|=\sqrt{\Gamma^*\Sigma^{*-1}}$ (see the sketch in Fig. 5). The right-hand side of Eq. (38) depends on $|\mathbf{k}|$ and H. It is sketched in Fig. 5 for several values of H (the graph for arbitrary H can be obtained by shrinking the graph for $H=1$ parallel to the $|\mathbf{k}|$ axis with coefficient H). At the critical thickness $H_{\rm crit}$, both graphs are tangential to each other. The abscissa at the point of tangency gives the neutral wave number $|\mathbf{k}|_{\rm ne}$. For fixed H and sufficiently small g, the constant Γ^* is also small. Equating tangents at the point of tangency, we obtain the following critical thickness and wave number:

$$H_{\rm crit}=\Sigma^*+2\left[\frac{2}{3}\frac{3+4\nu_f}{1-\nu_f}\Gamma^*\Sigma^{*3}\right]^{1/2},$$
$$k_{ne}=4\left[\frac{6(1-\nu_f)}{3+4\nu_f}\frac{\Gamma^*}{\Sigma^{*3}}\right]^{1/4}. \tag{40}$$

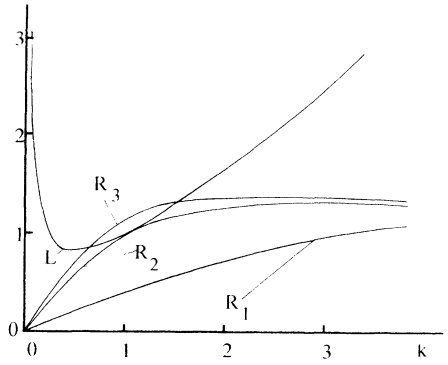

FIG. 5. The graphs of the accumulated energies of the film attached to the rigid substrate (R_1, R_2, and R_3 are the graphs for the subcritical, critical, and transcritical thicknesses, respectively).

Thus the corrections for small mass force is of order $g^{1/2}$ for the critical thickness, whereas for the neutral wave number k_{ne} it is of order $g^{1/4}$ (according to Refs. 23 and 25, for infinitely thick film $k_{ne} \sim g^{1/2}$).

Consider now an isotropic film of thickness H coherently attached to an infinitely thick isotropic deformable substrate. This case is more relevant to the study of epitaxial growth of nanofilms when elastic modules of the film and substrate are close in magnitude (see the warning in Sec. V). The observations of epitaxial growth[20] show that islanding begins with the corrugations which are much longer than the film thickness. According to Eq. (22), asymptotic formulas for the accumulated elastic energy at $h(=|\mathbf{k}|H)$ approaching infinity differ crucially depending on substrate rigidity. For the cases of (a) rigid ($\chi=\mu_f/\mu_s=0$) and (b) deformable ($\chi\neq 0$) substrates, one can find the following formulas:

$$\chi=0: \quad E^e_{\text{irreg}}-E^e_{\text{reg}} \sim h(T_n^2+T_t^2) , \tag{41a}$$

$$\chi\neq 0: \quad E^e_{\text{irreg}}-E^e_{\text{reg}} \sim \chi[(1-\nu_s)T_n^2+T_t^2] . \tag{41b}$$

Therefore, in the absence of mass forces, every crystalline layer coherently attached to a deformable substrate can always be destabilized by corrugations which have sufficiently long components. We denote by $\mathbf{k}^{0\chi}_{ne}$ the neutral wave vector of the surface corrugations in the case of negligible mass forces and substrate or relative rigidity χ. Then, Eqs. (22) and (41) give the following equation for the trenchlike pattern (provided $h^{0\chi}_{ne} \ll 1$):

$$\frac{2\pi}{|\mathbf{k}|^{0\chi}_{ne}}=\frac{\mu_s}{\mu_f}\frac{2\pi}{|\mathbf{k}|^{01}_{ne}} . \tag{42}$$

Equation (42) shows that the neutral wavelength of corrugation increases proportionally to the substrate rigidity. Thus, at arbitrary nonzero thickness each laterally unbounded film appears to be unstable with respect to sufficiently long corrugations. In other words, there is no critical thickness for solid films growing atop deformable substrates in the absence of mass forces. Mass forces, however, are most effective in suppressing the unstable corrugations having long wavelengths. That circumstance provides the change of obtaining nonvanishing critical thickness.

Following Nozières,[23] we take into account van der Waals forces acting on growing films. These forces strongly depend on the distance from the substrate; hence the acceleration g becomes a function of H. Combining Eqs. (12) and (42) we arrive at the following formulas for the critical wave number and thickness:

$$|\mathbf{k}|_{ne}=\left[\frac{\rho_f g}{\sigma}\right]^{1/2}=\frac{1-\nu_s}{2}\frac{T_n^2}{\sigma\mu_s} ,$$
$$\rho_f g(H_{\text{crit}})=\frac{(1-\nu_s)^2}{4}\frac{T_n^4}{\sigma\mu_s^2} . \tag{43}$$

The latter of Eqs. (43) has to be treated as the equation with respect to the unknown thickness H_{crit}. Solutions of this equation depend on the function $\rho_f g(H)$. Consider, for instance, the power dependence $\rho_f g(H)=WH^{-n}$, where W is a constant. Then we arrive at the following formula (it slightly generalizes the formulas of the critical thickness established earlier[23,26]):

$$H_{\text{crit}}=W^{1/4}\left[\frac{1-\nu_s}{2}\right]^{-2/n}\mu_s^{2/n}\sigma^{1/n}|T_n|^{-4/n} . \tag{44}$$

Equation (44) prompts us to conclude that the critical thickness tends to go to infinity as μ_s approaches infinity. However, this would not be a correct statement, since we have used the asymptotic formula (41b) while deriving (44) (the asymptotics is not uniform in the μ_s).

VIII. CONCLUSIONS

In the absence of surface tension a flat boundary of nonhydrostatically stressed elastic solids in always unstable with respect to "mass rearrangement." Some features of the instability in numerous phenomena certainly depend on specific circumstances such as the mechanisms of mass transport, physical and mechanical properties of the materials, existing force and thermal fields, etc. On the other hand, the occurrence of the instability is purely thermodynamic in nature and does not depend on these mechanisms. The instability allows to explain some recent experiments in the ^{4}He crystals under stress.[13] Also, it delivers opportunities to the theory of dislocation-free Stranski-Krastanov pattern of epitaxial growth.

There may exist two critical thicknesses associated with the instability in prestressed elastic films attached to a solid substrate. The first corresponds to the destabilization of flat films in favor of long parallel, periodic corrugations. For some types of stress, a second critical thickness exists, corresponding to the formation of another set of corrugations. The corrugations, then, produce a two-dimensional superlattice of rectangular islands rather than a one-dimensional lattice of trenches.

Attractive mass forces (i.e., those with positive acceleration g) always increase the static critical thickness of stressed solid films attached to the substrates. Both the critical thickness and its corrugation for gravity are detectable in experiments such as those described in Ref. 13.

[1]D. P. Woodruff, *The Solid-Liquid Interface* (Cambridge University Press, Cambridge, 1973).
[2]J. W. Christian, *The Theory of Transformations in Metals and Alloys* (Pergamon, Oxford, 1975).
[3]J. W. Martin and R. D. Doherty, *Stability of Microstructure in Metallic Systems* (Cambridge University Press, Cambridge, 1976).
[4]*Solids Far From Equilibrium,* edited by C. Godrèche (Cambridge University Press, Cambridge, 1991).
[5]M. A. Grinfeld, *Thermodynamic Methods in the Theory of Heterogeneous Systems* (Longman, Sussex, 1991).
[6]R. J. Asaro and W. A. Tiller, Metall. Trans. **3**, 1789 (1972).
[7]M. A. Grinfeld, Fluid Dyn. **22**, 169 91987); J. Nonlinear Sci. **3**, 35 (1993).
[8]P. Nozières, in Solids Far From Equilibrium, edited by C. Godrèche (Cambridge University Press, Cambridge).
[9]D. J. Srolovitz, Acta Metall. **37**, 621 (1989).
[10]L. B. Freund and F. Jonsdottir, J. Mech. Phys. Solids **41**, 1245 (1993).
[11]M. A. Grinfeld, Dokl. Akad. Nauk. SSSR **290**, 1358 (1986) [Sov. Phys. Dokl. **31**, 831 (1986)].
[12]M. Thiel, A. Willibald, P. Evers, A. Levchenko, P. Leiderer, and S. Balibar, Europhys. Lett. **20**, 707 (1992).
[13]R. H. Torii and S. Balibar, J. Low Temp. Phys. **89**, 391 (1992).
[14]J. Berrehar, C. Caroli, C. Lapersonne-Meyer, and M. Schott, Phys. Rev. B **46**, 13 487 (1992).
[15]B. Caroli, C. Caroli, B. Roulet, and P. W. Voorhees, Acta Metall. **37**, 257 (1989); P. H. Leo and R. F. Sekerka, *ibid.* **37**, 3119 (1989).
[16]A. Onuki, Phys. Rev. A **39**, 5932 (1989).
[17]W. J. Heidug, Geophys. Res. **21**, 909 (1991); W. K. Heidug and Y. M. Leroy, J. Geophys. Res. (to be published).
[18]H. Gao, J. Mech. Phys. Solids **39**, 443 (1991); Int. J. Solid Struct. **28**, 701 (1991).
[19]C. W. Snyder, B. G. Orr, D. Kessler, and L. M. Sander, Phys. Rev. Lett. **66**, 3032 (1991); B. J. Spencer, P. W. Voorhees, and S. H. Davis, *ibid.* **67**, 3696 (1991); B. J. Spencer, S. H. Davis, and P. W. Voorhees, Phys. Rev. B **47**, 9760 (1993); M. A. Grinfeld, J. Intellig. Mater. Syst. Struct. **4**, 76 (1993).
[20]D. J. Eaglesham and M. Cerullo, Phys. Rev. Lett. **64**, 1943 (1990); S. Guha, A. Madhukar, and K. C. Rajkumar, Appl. Phys. Lett. **57**, 2110 (1990); F. K. LeGoues, M. Copel, and R. M. Tromp, Phys. Rev. B **42**, 11 690 (1990).
[21]J. H. van der Merwe, J. Appl. Phys. **34**, 117 (1963); J. W. Matthews and A. E. Blakeslee, J. Cryst. Growth **27**, 118 (1974); G. H. Gilmer and M. H. Grabow, J. Met. **23**, 19 (1987); R. Bruinsma and A. Zangwill, Europhys. Lett. **4**, 1729 (1987).
[22]L. C. Stoop, Thin Solid Films **24**, 229 (1974); **24**, 243 (1974); D. Vanderbilt, O. L. Alerhand, R. D. Meade, and J. D. Joannopoulos, J. Vac. Sci. Technol. B **7**, 1013 (1989); E. Kasper and H. Jorke, *ibid.* **10**, 1927 (1992); J. Tersoff, Phys. Rev. B **43**, 9377 (1991).
[23]P. Nozières (unpublished).
[24]J. Grilhe, Acta Metall. Mater. **41**, 909 (1993).
[25]S. Balibar, D. O. Edwards, and W. F. Saam, J. Low Temp. Phys. **82**, 119 (1991); R. M. Bowley and P. Nozières, J. Phys. **2**, 433 (1992); R. M. Bowley, J. Low Temp. Phys. **89**, 401 (1992).
[26]M. A. Grinfeld, Europhys. Lett. **22**, 723 (1993).

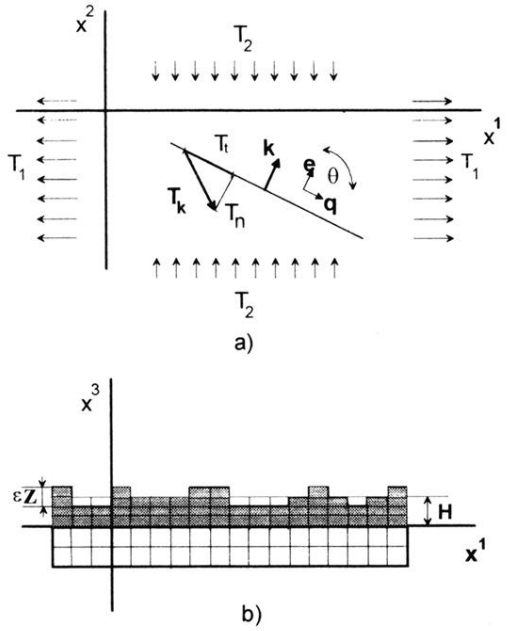

FIG. 2. The geometry of the corrugated film. (a) Top view. (b) Side view.